Scattering from a perfectly conducting plate using wire-grid and MoM with pulse basis functions

Tuan Phuong Dang
Department of Television and Control
Tomsk State University of Control Systems and Radioelectronics
Tomsk, Russia
dang.p.2213-2023@e.tusur.ru

Adnan F. Alhaj Hasan
Department of Television and Control
Tomsk State University of Control Systems and Radioelectronics
Tomsk, Russia
alkhadzh@tusur.ru

Talgat R. Gazizov
Department of Television and Control
Tomsk State University of Control Systems and Radioelectronics
Tomsk, Russia
talgat.r.gazizov@tusur.ru

***Abstract*—This paper analyzes the scattering characteristics from a solid perfectly conducting flat plate. Different plates with different incident plane waves are considered. Radar cross sections including the monostatic and bistatic ones are obtained and compared for all structures. The efficiency of using a developed wire grid code based on the method of moments with pulse basis functions is proved by comparing its results with those published in other works and obtained experimentally and numerically using the method of moments with different schemes and basis functions. It is revealed that the considered model and the code developed on its base can be effectively used in the future for modeling of complex wire grid and solid scatterers and even for creating new sparse ones based on the agreement found in the scattering field calculations.**

Keywords—Scatterer, wire-grid, method of moments, plate, pulse basis function, radar cross section.

I. INTRODUCTION

The development of new scattering structures has been of interest for a long time [1]. However, the electrodynamic modeling of such structures remains a challenging task. Moreover, their accurate modeling is of great importance in various fields including civilian as well as military applications [2, 3]. Since the 1960s, the wire grid (WG) modeling approach has received considerable attention and widespread use due to its ability to easily model structures of arbitrary geometry [4]. The appearance of advanced computing devices has also contributed to the further development of WG, allowing the simulation of more and more complex structures [5]. Despite its limitations, WG has demonstrated remarkable reliability in solving far-field problems when used to model perfectly conducting surfaces by replacing them with a grid of electrically connected thin wires [6, 7].

The method of moments (MoM) is known to be a common method for analyzing a variety of scattering structures [8, 9]. At the core of MoM lies the transformation of integral equations into a system of linear equations. This system is then solved numerically to determine the surface current and, subsequently, the scattered electromagnetic field. MoM can be used with many different types of meshing schemes such as basic pulse expansion point-matching function (PEPM), roof-top function expansion-line testing (RTLT) [7], and different types of basis functions such as the piecewise-sinusoidal (PWS) [10] and triangular (TBF) basis functions [11, 12].

This research was funded by the Ministry of Science and Higher Education of the Russian Federation project FEWM-2023-0014.

The choice of which basis function to use determines the accuracy, complexity, and required resources of MoM models. WG is usually used in conjunction with MoM to maximize the benefits of their advantages [4]. In particular, the use of MoM-based WGs with pulse basis functions (PBF) makes the structure segmentation process not only more understandable for complex structures and special cases such as dealing with junction current, but also easier in code implementation [13].

Recently, several models with different basis functions for scattering analysis have been developed. In particular, a model for analyzing wire scatterer using MoM with PBF was developed in [13]. The efficiency of this model was verified by comparing its results with those obtained using other numerical methods. However, it is reasonably to verify it comparing its results with those obtained by the same method either in different implementations or with different basis functions [14, 15]. This can be easily done when considering MoM because of the simpleness of its nature and the presence of numerous computer codes on its base. Furthermore, this model is expected to be used together with the optimal current grid approximation approach to create sparse WG scatterers, which increases the relevance of its verification. Moreover, such issue requires to verify this model not only by applying it to simple wire structures but also to increase the complexity of the considered structures starting from simple WG ones.

Therefore, in order to efficiently use this model for future modeling of scatterers and creating new sparse scattering structures it is an urgent task to verify its results of complex scattering structures including WG and solid ones. The aim of this work is to verify the results of the analysis of solid flat perfectly conducting plate using MoM-based WG model with PBF by comparing its results with those obtained using MoM with other schemes and basis functions. The results of scatterer plate analysis obtained in this study using a computer code based on the considered model with PBF are verified by comparing them with those obtained using MoM with PEPM [7], RTLT [7], TBF with adaptive multiscale MoM [12], and PWS [10], and experimentally [10].

This paper is organized as follows: Section II presents the parameters of the plate scattering structures under consideration and their equivalent WG models and gives detailed formulation of the incident plane waves with linear polarization used to excite them. Section III presents the obtained WG analysis using MoM with PBF results and verifies them through comparison with others. Section IV outlines general conclusions and directions for future work.

II. Equivalent WG Plates under Study

The flat rectangular perfectly conducting rectangular scattering plate under study is depicted in Fig. 1*a*. The plate is placed in the XOY plane, with the *z*-axis normal (orthogonal) to the plate surface. The origin of the coordinate system coincides with the plate center. Fig. 1*b* illustrates the aforementioned plate scatterer from Fig. 1a, approximated using WG in this work. The plate has edge lengths of L and W, while Δ is the edge length of all the WG cells, which equal to the length of each cell wire. Each of the four wires that form the WG cells is represented by one segment. This not only simplifies the structure segmentation process, but also agrees with the conditions and constraints summarized in [16] (especially that no basis function should pass the junction region).

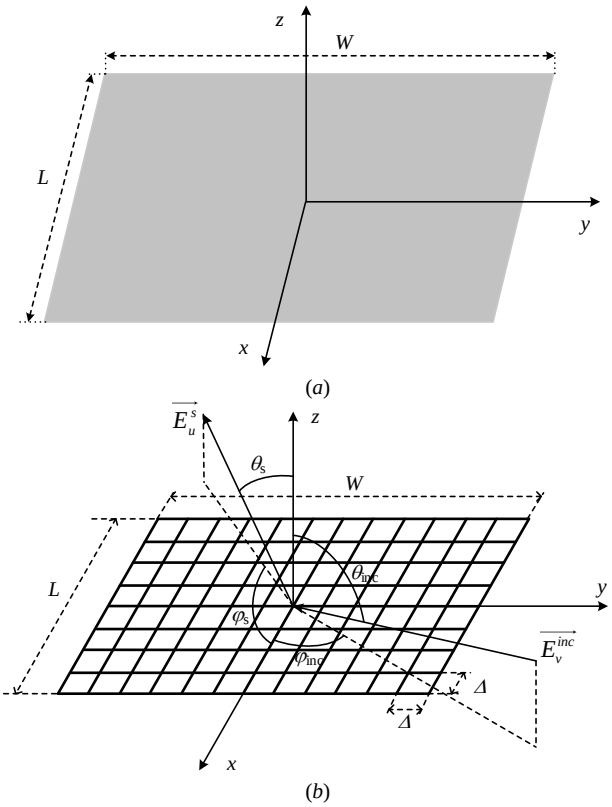

Fig. 1. Rectangular scatterer plate (*a*) and its equivalent WG structure (*b*).

When modeling such structures using WG, it is also important to consider the cell size. After all, it determines the accuracy of the analysis results and also affects the required computational cost. Researchers in [17] conducted a study to determine the most appropriate cell size for modeling a WG patch antenna. According to that study, the edges length of the WG cell is defined with respect to the wavelength (λ) [17] as

$$\frac{\lambda}{15} \geq \Delta \geq \frac{\lambda}{20} \tag{1}$$

In addition, the choice of wire radius (a) also affects the WG simulation results [18]. Here we apply a well-known rule for determining the wire radius, namely the Equal Area Rule (EAR). According to it, the cross-sectional circumference of a cylindrical wire as an edge in a WG with square cells must be equal to the length of that edge, as shown in Fig. 2.

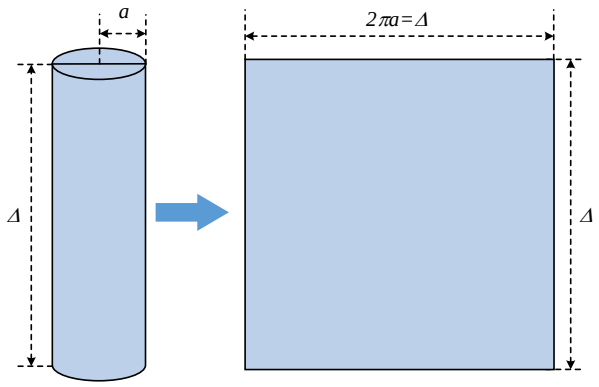

Fig. 2. Equal area rule explanation.

Based on that, the wire radius can be defined as

$$a = \frac{\Delta}{2\pi} \tag{2}$$

The plane wave in the spherical coordinate system can be written as [13]

$$E^{inc} = E_0 e^{-jk(x\sin\theta_{inc}\cos\varphi_{inc} + y\sin\theta_{inc}\sin\varphi_{inc} + z\cos\theta_{inc})} \tag{3}$$

where x, y, z are the center coordinates of the considered segment, k is wave number, and φ^{inc}, θ^{inc} are the azimuthal and elevation angles that determine the direction of the incident plane wave. The value of E_0 can be obtained as:

$$E_0 = \begin{cases} a_x \cos\theta_{inc}\cos\varphi_{inc} + a_y \cos\theta_{inc}\sin\varphi_{inc} - a_z \sin\theta_{inc}, \\ \qquad in\ case\ of\ \theta\ polarized\ plane\ wave, \\ -a_x \sin\varphi_{inc} + a_y \cos\varphi_{inc}, \\ \qquad in\ case\ of\ \varphi\ polarized\ plane\ wave, \end{cases} \tag{4}$$

where $a_{x,\,y,\,z}$ are calculated as:

$$\begin{aligned} a_x &= \Delta l_x / \Delta l, \\ a_y &= \Delta l_y / \Delta l, \\ a_z &= \Delta l_z / \Delta l, \end{aligned} \tag{5}$$

where $\Delta l_{x,\,y,\,z}$ are the vector projection of the vector $\overrightarrow{\Delta l}$ (which has the direction from the segment start to end points) on the Cartesian coordinate system axis, and Δl is length of segment.The radar cross section (RCS) can be calculated as

$$\sigma_{uv} = 4\pi R^2 \frac{\left|E_u^s\right|^2}{\left|E_v^{inc}\right|^2} \tag{6}$$

where R is the distance from the origin of the coordinate system to the point where the electrical field intensity is being calculated, E_v^{inc} is incident plane wave with v–polarization, and E_u^s is value of u component of the scattered far field.When the incident plane wave has a $v=\{\theta, \varphi\}$ polarization and the scattered field has a $u=\{\theta, \varphi\}$ component, the RCS can be defined as presented in Table I:

TABLE I. Index Notation of the Obtained RCS

		v	
		φ	θ
u	φ	$\sigma_{\theta\varphi}$	$\sigma_{\theta\theta}$
	θ	$\sigma_{\theta\varphi}$	$\sigma_{\theta\theta}$

The parameters of the considered scatterer plates are presented in Table II. In addition, the table also lists the type of schemes and basis functions that have been used for analyzing the same structures in other works.

TABLE II. ANALYSIS PARAMETERS OF THE CONSIDERED STRUCTURE

Structure	L, m	W, m	a, m	Δ, m	Cell No.	Type
S_1 [7]	1	1	0.01	0.067	15*15	PEPM/RTLT
S_2 [7]	0.5	0.5	0.01	0.0625	8*8	PEPM
S_3 [7]	1.5	1.5	0.01	0.068	22*22	PEPM
S_4 [7]	2	2	0.01	0.067	30*30	PEPM
S_5 [12]	1.1	1.1	0.01	0.069	16*16	TBF
S_6 [12]	2.1	2.1	0.01	0.069	32*32	TBF
S_7 [10]	2	3	0.016	0.1	20*30	PWS
S_7 [10]	2	3	0.016	0.1	–	experimentally

The cell numbers in Table II are determined using the mentioned above rules, while their values were not provided in considered works for verification. For all considered cases of these different scattering solid plates, the used linear polarized incident plane wave has a magnitude of 1 V/m, and a frequency f of 300 MHz. The direction of the excitation wave is perpendicular to the plane containing the plate, except in the case of monostatic and bistatic RCS calculations for structures S_5 and S_6, the plane wave had different directions.

III. VERIFICATION RESULTS

First, the RCS for S_1 obtained using MoM-based WG with PBF are compared with those obtained using MoM with RTLT and PEPM in [7] (Fig. 3 and 4). From Fig. 3 it can be seen that the maximum level of the $\sigma_{\varphi\theta}$ side lobe for S_1 when using MoM with RTLT is the highest (0.25 m^2), followed by its value with PBF (0.21 m^2), and then with PEPM (0.17 m^2). The maximum levels of the $\sigma_{\varphi\theta}$ main lobe match well. Fig. 4 show that for S_1, the maximum levels of the main lobe for $\sigma_{\varphi\theta}$ in the φ=0° plane and for $\sigma_{\theta\theta}$ in the φ=90° plane are the highest when using MoM with PBF (11.9 m^2), followed by their values with RTLT (11.3 m^2), and then with PEPM (10.6 m^2). This difference can be explained by the use of different base functions and plate models (WG and solid plates). In general, the obtained results agree well.

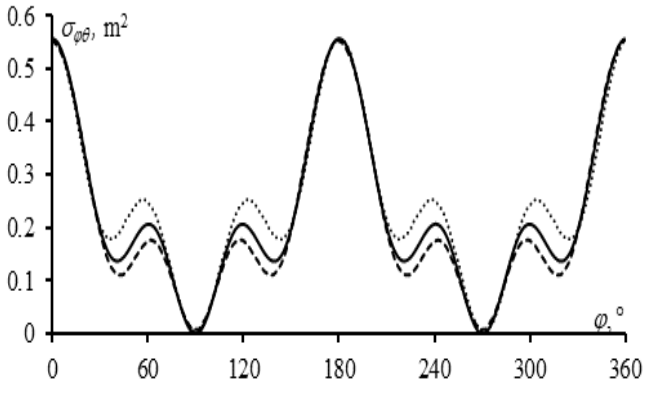

Fig. 3. Calculated $\sigma_{\varphi\theta}$ in plane θ=90° for S_1 using MoM with PBF (—), PEMP (--), and RTLT (···).

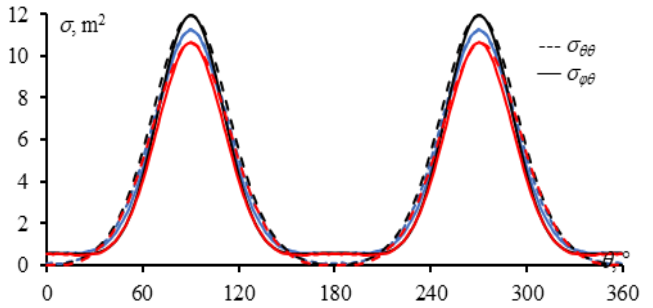

Fig. 4. Calculated $\sigma_{\varphi\theta}$ in φ=0° plane (—) and $\sigma_{\theta\theta}$ in φ=90° plane (---) for S_1 using MoM with PBF (black lines), PEMP (red lines) and RTLT (blue lines).

Next the RCS for S_1–S_4 obtained using MoM-based WG with PBF are compared with those obtained using PEPM in [7] (Fig. 5–7). Considering the calculated $\sigma_{\varphi\theta}$ in the θ=90° plane for S_3 and S_4, it can be seen that the difference between the compared results is quite large compared to the results of other structures (Fig. 5). However, the maximum levels of the obtained main lobes and their widths still match quite well. The obtained results for $\sigma_{\varphi\theta}$ in the φ=0° plane (Fig. 6), and for $\sigma_{\theta\theta}$ in the φ=90° plane (Fig. 7), coincide quite well with each other for all considered structures. In addition, it can be seen that as the size of the plate increases, the main lobe width decreases and scattered field amplitude rises, which agrees with the scattering theory.

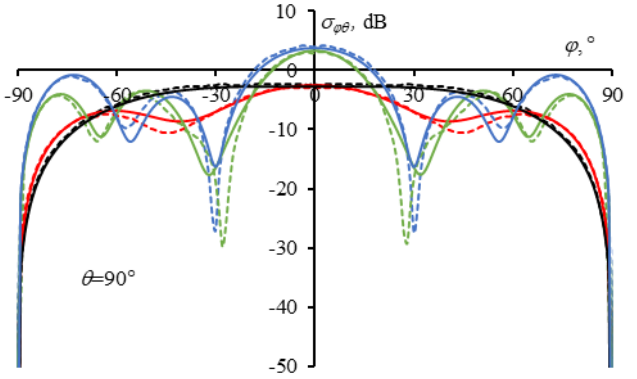

Fig. 5. Calculated $\sigma_{\varphi\theta}$ for S_1 (red), S_2 (black), S_3 (blue), S_4 (green) in the θ=90° plane using MoM with PBF (—), and PEMP (--).

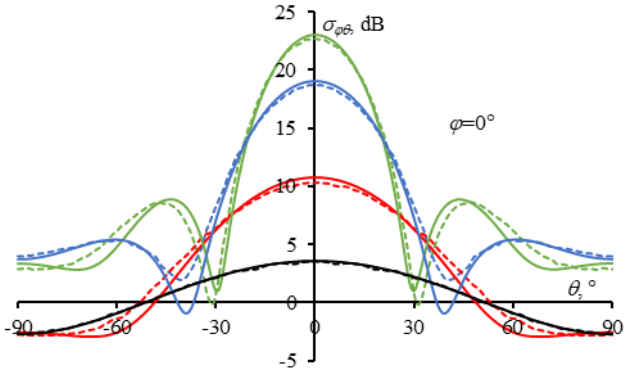

Fig. 6. Calculated $\sigma_{\varphi\theta}$ for S_1 (red), S_2 (black), S_3 (blue), S_4 (green) in the θ=0° plane using MoM with PBF (—), and PEMP (--).

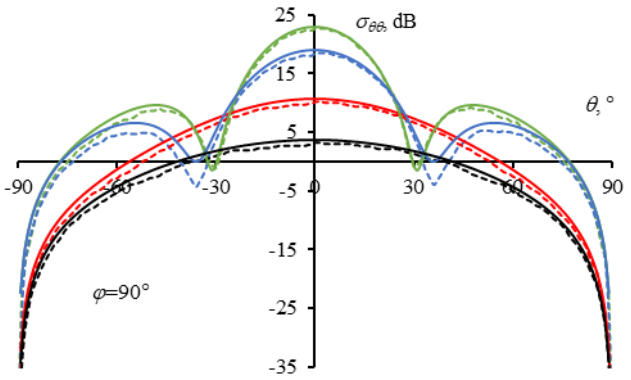

Fig. 7. Calculated $\sigma_{\theta\theta}$ for S_1 (red), S_2 (black), S_3 (blue), S_4 (green) in the θ=90° plane using MoM with PBF (—), and PEMP (--).

The maximum RCS deviations obtained by comparing the results using MoM-based WG with PBF and those in [7] are summarized in Table III. The analysis of the results shows that they differ maximumly for $\sigma_{\varphi\theta}$ by about of 12 dB, for $\sigma_{\varphi\theta}$ by about of 2.8 dB, and for $\sigma_{\varphi\theta}$ by about of 3.8 dB.

TABLE III. RCS MAXIMUM DEVIATION FOR S_1–S_4

	Deviation, dB			
Structure	S_1	S_2	S_3	S_4
$\sigma_{\varphi\theta}$ (θ=90°)	2	0.3	11	12
$\sigma_{\theta\theta}$ (φ=0°)	0.6	0.1	2.8	1
$\sigma_{\theta\theta}$ (φ=90°)	1	0.3	3.8	2

Next, the results of analyzing S_5 and S_6 scattering plates using MoM-based WG with PBF are compared with those obtained using MoM with TBF in [12]. The compared RCS using the earlier plane wave parameters are presented in Fig. 8 for S_5 and in Fig. 9 for S_6. From Fig. 8 it can be seen that the main lobe maximum level obtained using MoM with PBF is larger than with TBF by about of 0.82 dB, while from Fig. 9 – by about of 0.6 dB.

Next, to calculate the monostatic RCS for S_5, a θ polarized incident plane wave from different directions of φ_{inc}=90° and θ_{inc}=0, ..., 90° is used, consequently the scattering field has directions of φ_s=90° and θ_s=0, ..., 90°, respectively. The compared monostatic RCSs for S_5 are presented in Fig. 10.

After that, to determine the bistatic RCS for S_6, also a θ polarized incident plane wave from different directions of φ_{inc}=90° and θ_{inc}=0, ..., 90° is used, while the scattering field has a direction of φ_s=90° and θ_s=90°. The compared bistatic RCSs for S_6 are presented in Fig. 11. In overall, the compared results are in good agreement with each other.

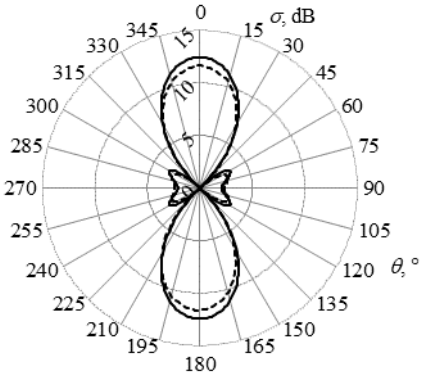

Fig. 8. RCS for S_5 using MoM-based WG with PBF (—) and TBF (---).

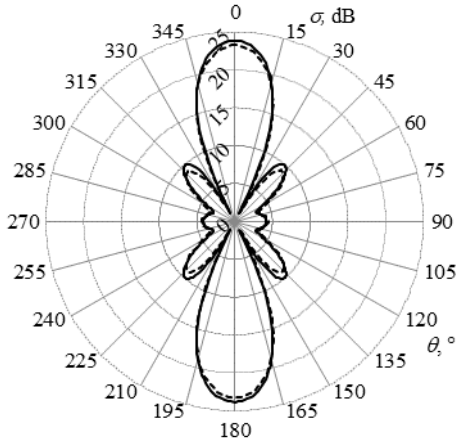

Fig. 9. RCS for S_6 using MoM-based WG with PBF (—) and TBF (---).

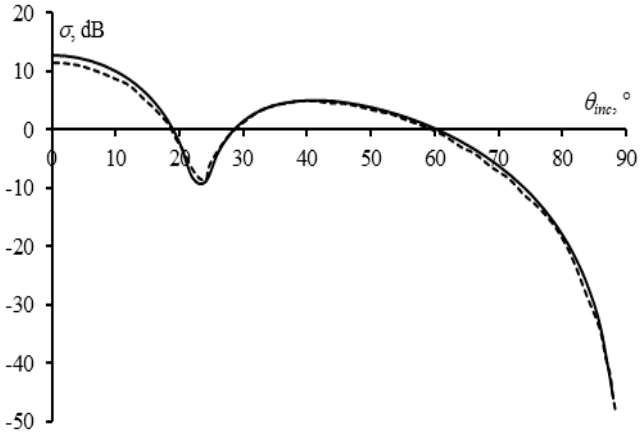

Fig. 10. Monostatic RCS for S_5 using MoM with PBF (—) and TBF (---).

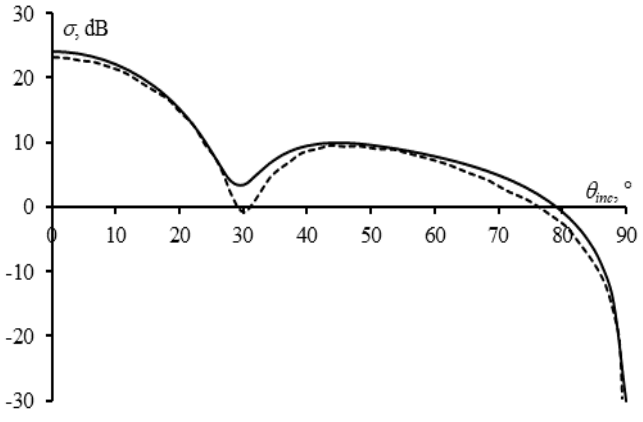

Fig. 11. Bistatic RCS for S_6 using MoM with PBF (—) and TBF (---).

Finally, the S_7 RCS results calculated using MoM-based WG with PBF are compared with those obtained numerically using MoM with PWS and experimentally in [10]. These RCS are obtained using the initial plane wave parameters mentioned in this work in the φ=0° (Fig. 12) and in the φ=90° (Fig. 13) planes. It is clearly visible that the MoM-based WG with PBF results and the measured ones coincide quite well. Moreover, it can be seen from Fig. 12 that MoM-based WG with PBF results are even closer to the actual measurement results than those calculated using MoM with PWS. All this prove the efficiency of using MoM-based WG with PBF for analyzing scattering plate structures and demonstrate the accuracy of its results.

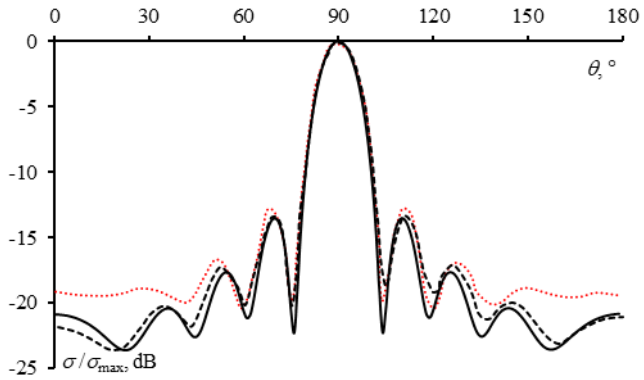

Fig. 12. Measured (--) and calculated $\sigma_{\theta\theta}$ results for S_7 in the φ=0° plane using MoM with PBF (—), PWS (···).

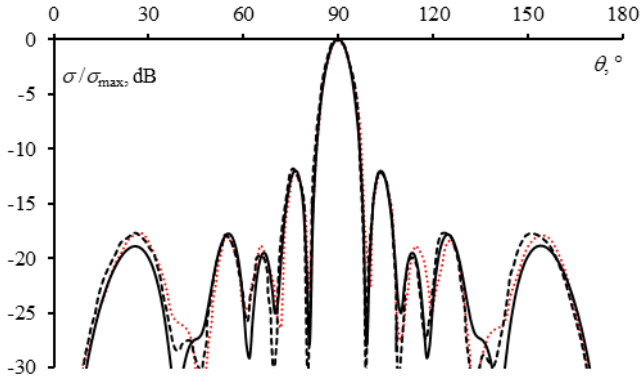

Fig. 13. Measured (--) and calculated $\sigma_{\theta\theta}$ results for S_7 in the φ=90° plane using MoM with PBF (—), PWS (···).

IV. Conclusion

This paper provides a comprehensive comparative analysis of the scattering characteristics from solid perfectly conducting flat plate. The main contribution of this work is to prove the efficiency of using a developed MoM-based WG code with PBF for analyzing such structures and demonstrate the accuracy of its results. To verify its results, they are compared with those obtained experimentally and numerically using MoM with other schemes and basis functions from other published works. The comparison showed good agreement in scattering field calculations. It was revealed that this model and the code developed on its base can efficiently be used for future modeling of complex WG and solid scatterers and creating new sparse scattering structures ones.

V. References

[1] N Stefanou, V Karathanos and A Modinos, “Scattering of electromagnetic waves by periodic structures,” in Journal of Physics: Condensed Matter, vol. 4, no. 36, Sep. 1991.

[2] X. Cao and X. Xu, “SAR image simulation with high fidelity of scattering characteristics for typical buildings,” 2023 IEEE Conference on Antenna Measurements and Applications (CAMA), Genoa, Italy, 2023, pp. 1020–1024, doi: 10.1109/CAMA57522.2023.10352812.

[3] Moosmüller, Hans, et al. “Scattering cross-section emission factors for visibility and radiative transfer applications: Military vehicles traveling on unpaved roads,” Journal of the Air & Waste Management Association, vol. 55, pp. 1743–1750, Nov. 2005.

[4] J. Richmond, “A wire-grid model for scattering by conducting bodies,” in IEEE Transactions on Antennas and Propagation, vol. 14, no. 6, pp. 782–786, November 1966, doi: 10.1109/TAP.1966.1138783.

[5] A. Rubinstein, F. Rachidi and M. Rubinstein, “On wire-grid representation of solid metallic surfaces,” in IEEE Transactions on Electromagnetic Compatibility, vol. 47, no. 1, pp. 192–195, Feb. 2005, doi: 10.1109/TEMC.2004.838230.

[6] K. S. H. Lee, L. Marin and J. P. Castillo, “Limitations of wire-grid modeling of a closed surface,” in IEEE Transactions on Electromagnetic Compatibility, vol. EMC-18, no. 3, pp. 123–129, Aug. 1976, doi: 10.1109/TEMC.1976.303482.

[7] K. Mahadevan, H. A. Auda and A. W. Glisson, “Scattering from a thin perfectly-conducting square plate,” in IEEE Antennas and Propagation Magazine, vol. 34, no. 1, pp. 26–32, Feb. 1992, doi: 10.1109/74.125886.

[8] D. R. Wilton, “History of developments leading to the method of moments,” 2018 International Applied Computational Electromagnetics Society Symposium (ACES), Denver, CO, USA, 2018, pp. 1–2, doi: 10.23919/ROPACES.2018.8364227.

[9] D. Olcan, J. Petrovic and B. Kolundzija, “Machine Learning for 2-D Scattering Analysis using Method of Moments,” 2020 IEEE International Symposium on Antennas and Propagation and North American Radio Science Meeting, Montreal, QC, Canada, 2020, pp. 1985–1986, doi: 10.1109/IEEECONF35879.2020.9330266.

[10] Nan Wang, J. Richmond and M. Gilreath, “Sinusoidal reaction formulation for radiation and scattering from conducting surfaces,” in IEEE Transactions on Antennas and Propagation, vol. 23, no. 3, pp. 376–382, May. 1975, doi: 10.1109/TAP.1975.1141080.

[11] H. Chao, B. Strait and C. Taylor, “Radiation and scattering by configurations of bent wires with junctions,” in IEEE Transactions on Antennas and Propagation, vol. 19, no. 5, pp. 701–702, September 1971, doi: 10.1109/TAP.1971.1140021.

[12] Chaowei Su and T. K. Sarkar, “Adaptive multiscale moment method (AMMM) for analysis of scattering from perfectly conducting plates,” in IEEE Transactions on Antennas and Propagation, vol. 48, no. 6, pp. 932–939, June. 2000, doi: 10.1109/8.865226.

[13] P. T. Dang, A. F. Alhaj Hasan and T. R. Gazizov, “Analyzing the wire scatterer using the method of moments with the pulse basis functions,” XXVII International Conference 2024 Wave electronics and its application in information and telecommunication systems (WECONF), Saint-Petersburg, Russia, 2024. To be published.

[14] IEEE Std 1597.1–2008. Standard for validation of computational electromagnetics computer modeling and simulation. Part 1, 2. – IEEE Standard, 2008. – 41 p.

[15] IEEE Std 1597.2–2010. Recommended practice for validation of computational electromagnetics computer modeling and simulations. – IEEE Standard, 2010. – 124 p.

[16] P. T. Dang, A. F. Alhaj Hasan and T. R. Gazizov, “Notes on the analysis of crossed wire scatterers with junction by a fast MoM-based code with pulse basis functions,” 8th International Conference on Information, Control, and Communication Technologies (ICCT–2024), Vladikavkaz, Russian Federation, 2024. To be published.

[17] L. Inclán-Sánchez, “Performance evaluation of a low-cost semitransparent 3D-printed mesh patch antenna for urban communication applications” Electronics, vol. 13, no. 1. pp. 153, 2024, doi: 10.3390/electronics13010153.

[18] A. Rubinstein, F. Rachidi and M. Rubinstein, “On wire-grid representation of solid metallic surfaces,” in IEEE Transactions on Electromagnetic Compatibility, vol. 47, no. 1, pp. 192–195, Feb. 2005, doi: 10.1109/TEMC.2004.838230.